

Tidal Dissipation on Titan

FRANK SOHL

Institut für Geophysik, Universität Kiel, Olshausenstrasse 40–60, D-24098 Kiel, Germany

WILLIAM D. SEARS*

Department of Planetary Sciences, Lunar and Planetary Laboratory, University of Arizona, Tucson, Arizona 85721

AND

RALPH D. LORENZ†

Unit for Space Sciences, University of Kent, Canterbury, United Kingdom
E-mail: rlorenz@lpl.arizona.edu

Received May 13, 1994; revised December 13, 1994

Tidal dissipation may constrain the nature of the surface and interior of Titan. Provided the surface of Titan is covered by satellite-wide hydrocarbon seas and oceans, the solid body of Titan would have to respond not only to the external tidal disturbance potential but also to the loading and shifting weights of liquids on the surface. To estimate the tidal response of Titan's interior which is assumed to be differentiated into a crust–mantle–core structure, several endmember-type models have been considered, each of them constrained by Titan's mass and radius and consistent with either a volatile-rich or a volatile-poor evolution of the satellite. The dissipation rates as a consequence of the inelastic response of Titan's interior to body and loading tides have been computed from the imaginary parts of complex Love numbers and mass load coefficients. Additionally, a new analytical model of bottom frictional dissipation as a consequence of tidal currents in a global ocean is presented and is shown to compare well with a numerical model for both the radial and libration components of the ocean tide. In contrast to the solid volatile-poor interior structure, the volatile-rich interior contains an internal liquid ammonia–water region overlain by an icy shell, thereby mechanically decoupled from the deep interior. While the latter produces higher tidal dissipation rates than the former due to greater shell flexibility, the greater motion of the ocean floor accordingly induces smaller ocean currents, and hence much lower ocean dissipation rates for the volatile-rich scenario. The resultant total dissipation rates have been compared to those required to damp Titan's orbital eccentricity over the age of the Solar System. While the highly dissipative

volatile-rich interior requires a time constant of orbit circularization of only about half this time period, the volatile-poor interior structure would allow restrictions on the minimum ocean depth and on ocean composition. Consequently, the volatile-rich scenario seems inconsistent with a primordial origin of the orbit eccentricity. This suggests Titan's interior may be rigid and that there is no global ocean. Alternatively, the eccentricity of the orbit may have a more recent origin. It is, however, also conceivable that the thermal history could have been governed by more rapid interior cooling in the past, thereby notably diminishing the amount of solid dissipation in the deep interior. © 1995 Academic Press, Inc.

INTRODUCTION

Tidal dissipation on Titan has been a matter of interest for some time: before the Voyager encounter with Titan, the orbital eccentricity of the satellite had been noted and was difficult to explain in the presence of dissipation in its icy body. The issue became considerably more complicated when it was realized that there could be extensive bodies of liquid on the surface. Sagan and Dermott (1982) computed dissipations in global methane oceans and found that tidal dissipation should have damped the eccentricity to a small value over the age of the Solar System, unless the oceans either were not present or were deeper than 400 m. This conclusion was compatible with early observations and photochemical models of Titan's atmosphere, but more recent modeling and radar and infrared study of Titan's surface argue against a deep global ocean.

An additional complication has come to light in recent years. Radar measurements by Muhleman *et al.* (1992),

* Now at: MS 183-501, Jet Propulsion Laboratory, 4800 Oak Grove Drive, Pasadena, California 91109.

† Now at: Department of Planetary Sciences, Lunar and Planetary Laboratory, University of Arizona, Tucson, Arizona 85721.

tracking a radar “bright spot” on Titan’s disk, suggest that the rotation of Titan is not quite synchronous, but has a period of 15.911 days, or 0.82 hr shorter than the orbital period. Sears *et al.* (1993) have since shown that such a supersynchronous rotation is stable, due to the eccentricity of the orbit, if Titan has no significant tidal bulge. Such a bulge big enough to capture Titan into synchronous rotation could be, for example, a “slab” 1 km thick and 100 km across, or, similarly, a “continent” 100 m thick and 350 km across (Greenberg and Weidenschilling 1984, Sears *et al.* 1993). On the other hand, observations of Titan in the IR methane windows show light-curve variations which are consistent with synchronous rotation (Griffith 1993) and the latest IR data from Lemmon *et al.* (1995) constrain rotation to be within 0.6 hr of synchronous, or within about 0.15 hr of synchronous if they add in older published IR observations.

The question of Titan’s rotation is an interesting one, but is beyond the scope of this paper. Here we confine ourselves to considering the eccentricity of Titan’s orbit, which is beyond question, and attempt to reconcile this eccentricity with the tidal dissipation in Titan’s interior and in any oceans that may lie on its surface. We compute the tidal dissipation in Titan’s interior, using what we hope are plausible physical models. Although observational evidence cited above is inconsistent with a global ocean, for the purpose of computing dissipation in liquids due to bottom friction, we do assume the oceans are global. The rate of change of orbital energy due to tidal dissipation is compared with that required to damp the orbital eccentricity from reasonable values over the age of the Solar System. The corresponding implications for the origin of Titan’s eccentricity are discussed.

TIDAL ENVIRONMENT ON TITAN

Titan orbits Saturn at a mean distance of 1.22 million km, with an orbital period of 15.945 days. The orbit, however, has a marked eccentricity $e = 0.029$. This has two effects. First, the sub-Saturn point on Titan oscillates in longitude (i.e., there is a geometrical libration). Second, as the Titan–Saturn distance changes, the magnitude of the tidal potential varies by a factor of $3e$, or 9%. The parameters of the system are summarized in Table I.

The movement of the sub-Saturn point, and hence the tidal potential field attached thereto, may be calculated as follows. The inertial direction of Saturn from Titan is obtained by integrating the following equation for rate of change of true anomaly ν ,

$$\dot{\nu} = \sqrt{\frac{GM_S}{p^3} (1 + e \cos \nu)^2}, \quad (1)$$

where GM_S is the gravitational constant times the mass

TABLE I
Global Parameters of Titan

Parameter	Value
Mean surface radius R_T , km	2575
Global mass M_T , kg	1.346×10^{23}
Planetocentric constant GM_T , $\text{km}^3 \text{s}^{-2}$	8978.2
Surface gravity g_s , m s^{-2}	1.35
Mean density $\bar{\rho}$, kg m^3	1881
Rock to ice ratio (by mass),	~55:45
Orbital semimajor axis a , km	1.2208×10^6
Free eccentricity e	0.0292
Mean orbital motion n , s^{-1}	4.56×10^{-6}
Period of revolution τ_{rev} , d	15.945
Period of rotation τ_{rot} , d	15.911 – 15.945
Surface pressure p_s , Pa	1.496×10^5
Surface temperature T_s , K	94
Surface heatflow estimate q_s , W m^{-2}	$\sim 6 \times 10^{-3}$
Hydrocarbon ocean density σ , kg m^{-3}	650

References: Burns 1986, Morrison *et al.* 1986, Schubert *et al.* 1986, Thomas 1991, Muhleman *et al.* 1992; Stevenson 1992.

of Saturn, $GM_S = 3.79 \times 10^{16} \text{ m}^3 \text{ sec}^{-2}$, $p = a(1 - e^2)$ is the semilatus rectum of the orbit, and a is the semimajor axis. The direction of Saturn relative to a fixed point on Titan’s equator is simply the difference between ν and the longitude of the point λ_p at periapsis passage, viz.

$$\lambda = \nu - \omega \cdot t - \lambda_p, \quad (2)$$

where ω is the rotation rate of Titan.

This movement of the sub-Saturn point is shown in Fig. 1 for the synchronous and nonsynchronous cases.

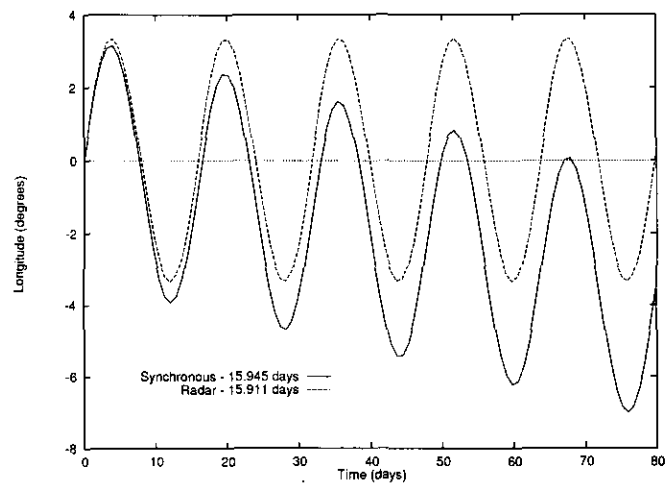


FIG. 1. Longitude variation over time of the sub-Saturn point on Titan. Both the synchronous (15.945 days) and nonsynchronous (15.911 days) rotation cases are shown.

For the nonsynchronous case there is a drift of one rotation approximately every 20 years superimposed on the libration. Hereafter, we will assume synchronous rotation. The maximum angular speed of the sub-Saturn point is approximately

$$\sqrt{\frac{GM_S}{a^3}} \left(2e + \frac{5}{2}e^2 + 3e^3 \right)$$

or 1.58×10^{-5} degrees per second, equivalent to a speed of 0.7 m sec^{-1} at the equator. This was obtained by differentiation of the equation of the center in Danby (1989).

The tidal acceleration β at a point on Titan's surface is given by

$$\beta = \frac{3GM_S R_T}{r^3} \sin(2\Theta), \quad (3)$$

where Θ is the angle between the point under consideration and the sub-Saturn point. If instantaneous zero longitude is defined as that of the sub-Saturn point, then $\cos(\Theta) = \cos \Gamma \cos \lambda$, where Γ is the latitude of the point. The variation in magnitude of the tide throughout the orbit manifests itself in the r^3 term in Eq. (3) with r given by

$$r = \frac{p}{1 + e \cos \nu}. \quad (4)$$

The libration is manifested by motion of the sub-Saturn point over the surface during the orbit. To a first approximation, the resulting difference between Titan's principal equatorial and polar radii upon tidal and rotational forcing can reach up to 509 m in the limit of homogeneous density, provided that Titan is near hydrostatic equilibrium (Zhar'kov *et al.* 1985).

More formally the external tidal disturbance potential Φ^e acting on Titan can be represented in terms of an infinite sum of zonal spherical harmonics according to

$$\Phi^e = \frac{GM_S}{a} \sum_{l=2}^{\infty} \left(\frac{R}{a} \right)^l P_l^0(\cos \Theta), \quad (5)$$

where R is radial distance from Titan's center of mass and M_S is the mass of Saturn. Upon converting coordinates from spherical to Keplerian elements, Kaula (1966) gave a general development of Eq. (5) which includes the effects of orbital inclination and eccentricity as well as the satellite's rotation. Since the length of Titan's semimajor axis is several orders of magnitude larger than Titan's surface radius, the most important perturbation is expected to arise from the term of lowest order in R/a , which is the first term of Eq. (5). A convenient representation of

such an external tidal disturbance potential has been given recently by Segatz *et al.* (1988) for a synchronously rotating satellite in a zero inclination orbit of low, but nonzero, eccentricity. Our model Titan fits these assumptions as well; thus Eq. (5) can be replaced by

$$\Phi^e \approx \Phi_2^e = (nR_T)^2 e (3P_2^0(\cos \theta) \cos nt + 2P_2^1(\cos \theta) \cos \phi \sin nt), \quad (6)$$

where θ is the colatitude, ϕ is longitude, e is orbital eccentricity, and t is time. Note that colatitude and longitude are measured relative to the average subsaturnian point (for θ) and Titan's trailing orbit tangent (for ϕ) which causes the $\theta = 0$ "pole" to lie in the orbit plane. This is different than the system used in Eqs. (1) through (4), which places the pole on the rotation axis. The first term in Eq. (6) then represents the radial tide due to the varying distance of Saturn, and the second term accounts for the libration component of the tide. The resulting tidal bulge can be viewed as circling Titan with angular velocity $n/2$ and with amplitude ranging from $1.5(nR_T)^2 e$ to $3.2(nR_T)^2 e$ at its equator (Segatz *et al.* 1988). Figure 2a shows the motion of the equatorial bulge over time. Note that we are using *only* the time variable portions of the potential and ignoring the time average component, since only the time varying portions can produce dissipation.

In order to gain a more precise estimate of the average size of the tidal bulge implied by Eq. (6), it is useful to rewrite it as

$$\Phi^e \approx \Phi_2^e = (nR_T)^2 e \left(\left(\frac{3}{8} + \frac{3}{2} \cos \phi \right) \cos(2\theta - nt) + \left(\frac{3}{8} - \frac{3}{2} \cos \phi \right) \cos(2\theta + nt) + \frac{3}{4} \cos nt \right). \quad (7)$$

The first term on the right-hand side is the primary eastward-moving component, the second is a much smaller westward-moving component, and the final term is a motionless time-varying component. Figure 2b will help to visualize these moving components. From Eq. (7) it is obvious where Segatz *et al.* (1988) obtain the angular velocity of the potential—it is simply the velocity of the primary component.

There are three direct effects and one indirect effect of this time-varying tidal potential. First the solid body of Titan responds to the potential. Second, liquids on the surface similarly respond to attain nearly hydrostatic equilibrium with the potential field. This introduces the indirect effect, namely that of loading tides: the solid body of Titan in turn responds to the loading of the shifting weight of liquids on the surface.

The third direct effect is the response of the atmosphere to the tidal potential (Lorenz 1992a). This may lead to significant tidal winds. Since dissipation scales with density, the atmospheric dissipation is approximately 100

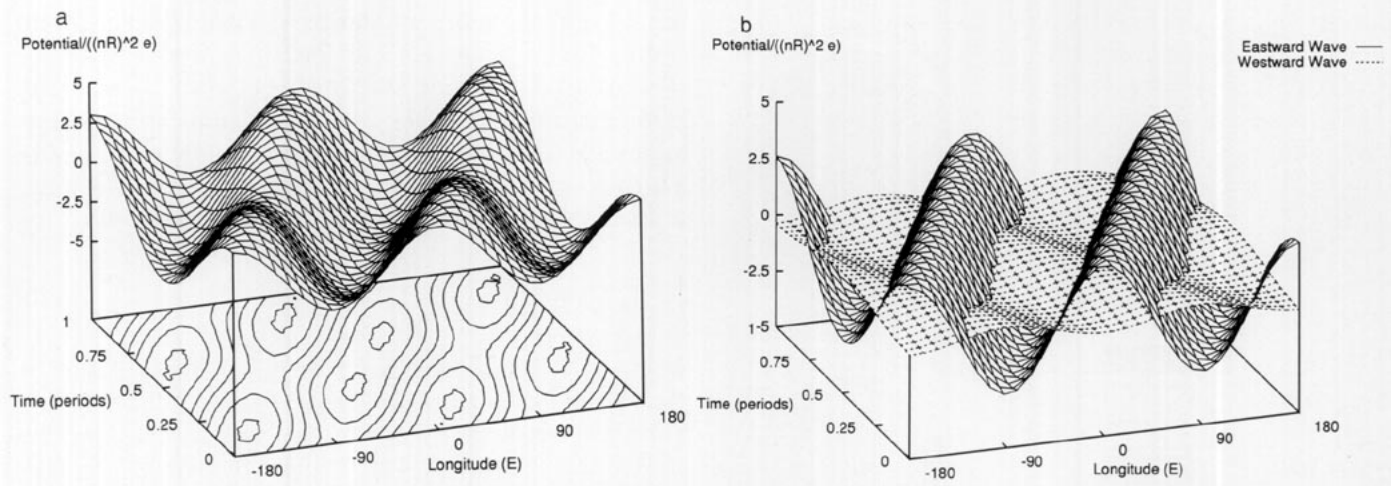


FIG. 2. (a) Schematic of the tidal potential showing the movement of the bulge around the equator over time. It can be viewed as a two-lobed bulge of varying amplitude moving around Titan. Contours are one (1) unit apart. (b) The primary eastward- and westward-moving components of the equatorial tidal potential, showing the motions over time. Compare with (a) to see the relative contributions to the total.

times smaller than for a liquid ocean. Further, taking the “depth” of the atmospheric ocean as equal to one scale height $H = R_0 T / g_s M$, where R_0 is the universal gas constant $8.314 \text{ J K}^{-1} \text{ mol}^{-1}$ and M is the mean molecular mass $0.028 \text{ kg mol}^{-1}$, gives a depth of order 20 km for Titan. Thus the “atmospheric ocean” is deep, and by virtue of its low density, has a very low dissipation, which we do not consider further.

INTERIOR MODELS OF TITAN

Simply due to the existence of Titan’s substantial nitrogen atmosphere, we suspect that the bulk composition of the planetesimal population that formed the satellite was rich in volatile components. Furthermore, accretional heating is believed to have been the primary driving force for internal differentiation into a rocky core and an icy mantle accompanied by partial outgassing of the interior, thus forming an early atmosphere around Titan shortly after accretion was completed. Today there may be a slight residual loss of accretional energy, estimated at $2.8 \times 10^{29} \text{ J}$ by Schubert *et al.* (1986), and energy of differentiation, which is about 12% of the accretional energy. However, the present contribution of these sources is difficult to estimate and is beyond the scope of the present paper.

Moreover, while discussing Titan’s origin it must be mentioned that the early evolution of almost all saturnian satellites may have been seriously affected by the presence of liquid water and the resulting extensive resurfacing (Squyres and Croft 1986). This leads one to believe that volatile components appear in roughly cosmic abundances in Titan’s interior and to argue for volatile ratios as high as $\text{NH}_3/\text{H}_2\text{O} = \frac{1}{8}$ and thus $\text{NH}_3/\text{CH}_4 \approx 1$ within

Titan (Stevenson 1992). Depending on the precise amount of volatiles incorporated into the icy mantle, the actual radiogenic heating rate in the core, and the effectiveness of the heat transfer to the surface, an existing ammonia-rich liquid water layer may have formed beneath Titan’s icy crust and may have survived to the present day. Owing to the variation in pressure and temperature throughout the interior, the icy mantle is likely to be subdivided into several water-ice layers such as ice I, ice II, ice V, and ice VI, each of them more or less contaminated by volatile species such as CH_4 and NH_3 (Stevenson 1992). Nevertheless, the interior of Titan is as much a mystery at present as the surface (Lunine 1993, Lorenz 1993); thus we consider three endmember-type models of Titan’s present interior structure to estimate the tidal response. These models are constrained by the global properties of Titan such as its mass of $1.35 \times 10^{23} \text{ kg}$ and its mean surface radius of 2575 km (Thomas 1991) that allows one to infer Titan’s mean density with confidence.

The uniform model **A** of Titan shown in Fig. 3 is based on a mean density $\bar{\rho}$ of 1881 kg m^{-3} and an approximate ice mass fraction f_{ice} of 0.45 according to the relation

$$f_{\text{ice}} = 1 - \frac{1 - \rho_{\text{ice}}/\bar{\rho}}{1 - \rho_{\text{ice}}/\rho_{\text{rock}}}, \quad (8)$$

where $\rho_{\text{ice}} = 1200 \text{ kg m}^{-3}$ is high-pressure ice density and $\rho_{\text{rock}} = 3500 \text{ kg m}^{-3}$ is anhydrous rock density (Schubert *et al.* 1986). Since model **A** cannot account for the complex thermal history Titan might have undergone, we further use two highly differentiated interior models such as those recently suggested by Stevenson (1992) for a volatile-rich and volatile-poor evolution of the satellite. Again,

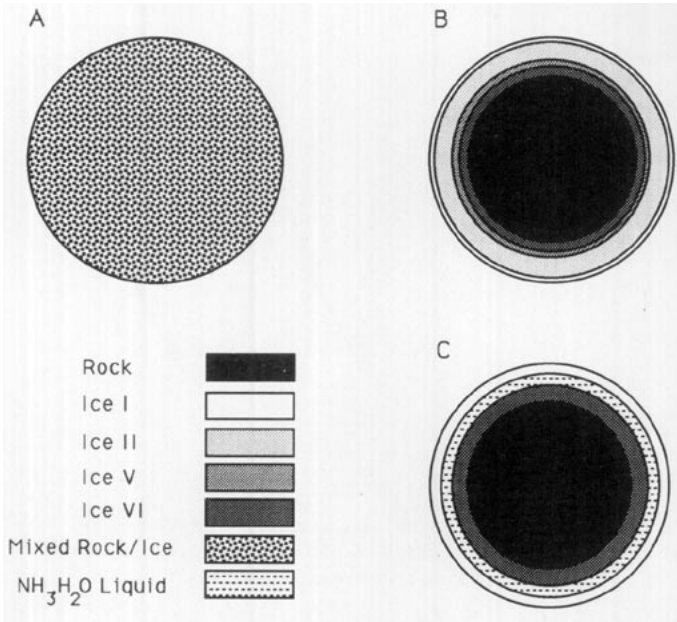


FIG. 3. The interior models used. Model A—a homogeneous rock/ice sphere. Model B—a differentiated volatile-poor model, with a rock core and layers of different ice phases. Model C—a differentiated volatile-rich model, with a rock core and a layer of ammonia–water liquid between ice layers.

see Fig. 3. Model B applies to the volatile-poor scenario that is similar to the development of Ganymede and Callisto in the jovian system. Outside a rocky core of 1900 km radius, a 200-km-thick ice VI zone overlain by 75 km of ice V and 300 km of ice II with a 100-km ice I crustal layer are assumed. In contrast to this model, incorporating a significant fraction of NH_3 and CH_4 leads to the volatile-rich scenario, referred to as model C, wherein water–ice is replaced with ammonia–water ice, except in a 300-km thick internal $\text{NH}_3\text{--H}_2\text{O}$ ocean beneath a 150-km-thick crustal layer (Cynn *et al.* 1989). The high-pressure ice zone situated between the internal ocean and the rocky core is most likely made of ice VI (Stevenson 1992).

As a consequence of Titan's low surface temperature, $T_s = 94 \text{ K}$, the outermost portion of its ice I crust is believed to form a rigid, conductive lithosphere extending to a critical depth at which subsolidus creep may be activated due to the temperature increase with depth. Likewise, such a transition in rheological behavior of the crust layer represents the conversion from purely elastic material behavior in the absence of strain energy dissipation to viscoelastic, and hence dissipative, material behavior upon tidal forcing. The depth at which that peculiar transition would be reached is believed to be related to tidal frequency and the depth-dependent ratio between local temperature and melting temperature T_m given by (Ellsworth and Schubert 1983)

$$T_m(p) = 273 + (0.0075 + 1.4 \times 10^{-11}p) \times (1.0 - 10^{-5}p) \quad (9)$$

in the case of ice I, where $p = \rho_l q_s z$ is lithostatic pressure in pascals, ρ_l is local density, and z is depth. Assuming a steady-state temperature field in the absence of heat sources the lithospheric temperature then becomes

$$T(z) = T_s + \frac{q_s}{k} z, \quad (10)$$

where q_s is Titan's surface heat flow estimated at $6 \times 10^{-3} \text{ W m}^{-2}$ (Stevenson 1992) and $k = 2.2 \text{ W m}^{-1} \text{ K}^{-1}$ is a thermal conductivity appropriate for ice I. Taking the critical temperature at which subsolidus creep becomes effective as $0.6 T_m$ (Ellsworth and Schubert 1983) and disregarding the frequency dependence of rheology we finally obtain $z = 25 \text{ km}$ as the critical minimum transition depth above which dissipation of tidal strain energy is believed to be absent.

Underneath such a rheological lithosphere, the buoyancy of warm ice may be sufficient to overcome viscosity, possibly leading to solid-state convection of Titan's lower crustal portion overlying the internal ammonia–water ocean in the volatile-rich case and therefore giving rise to the possible existence of thermal boundary layers attached to the top and the bottom of the convecting region. The stability against convection of the crust layer beneath the rheological lithosphere may be parameterized by the Rayleigh number according to (Peltier 1989)

$$Ra = \frac{\rho g \alpha}{\eta \kappa K} b^4 (q_s + \rho \varepsilon_{\text{tide}} b), \quad (11)$$

where $\kappa = K/\rho c_p$ and density $\rho = 1000 \text{ kg m}^{-3}$, specific heat capacity $c_p = 1000 \text{ J kg}^{-1} \text{ K}^{-1}$ (Lupo and Lewis 1979), thermal expansivity $\alpha = 5 \times 10^{-5} \text{ K}^{-1}$, thermal conductivity $K = 2.2 \text{ W m}^{-1} \text{ K}^{-1}$ (Turcotte and Schubert 1982), dynamic viscosity $\eta = 1 \times 10^{17} \text{ Pa}$ (Stevenson 1992), and surface gravity is $g_s = 1.35 \text{ m sec}^{-2}$. The second term in parentheses, wherein $\varepsilon_{\text{tide}}$ is specific tidal dissipation rate and b is shell thickness beneath the rheological lithosphere, represents the contribution to Titan's total surface heatflow as a consequence of tidal distortion of the crust layer. When Ra exceeds a critical value of order 10^3 the layer becomes unstable with respect to convection. Provided the second term contributes only negligible amounts and given the crust thickness is 100 to 150 km, the uppermost 25 km of which represents the immobile rheological lithosphere, we find Ra in the range 3×10^4 to 2×10^5 , implying modest convective circulation of crustal material efficiently cooling the ammonia–water ocean from above. Whether this convection manifests itself as "hot spots" or tectonically recycles the whole crust

as on Earth will be an interesting question that we hope the Cassini mission will be able to resolve.

The range of material dissipation factors pertaining locally to each layer of various ice polymorphs will depend on the contributions from individual attenuation mechanisms upon tidally induced shear deformation (cf. Poirier 1982). With respect to the probably high homologous temperature at which Titan's interior is operating at present (Stevenson 1992), we may concentrate on a steady-state mechanism of attenuation by attaching a viscoelastic Maxwell rheological model to the interior structure of models **B** and **C**. Then the material dissipation factor Q_μ is given by

$$Q_\mu = \frac{\rho_l \nu_{\text{ice}}}{\mu_{\text{ice}}} n, \quad (12)$$

where n is mean motion, ρ_l is local density of each ice polymorph, ice rigidity μ_{ice} is taken as 3.5 GPa (Gammon *et al.* 1983), and kinematic viscosity ν_{ice} is obtained according to (Ellsworth and Schubert 1983)

$$\nu_{\text{ice}} = 0.139 \times \exp(7214/T) \quad (13)$$

as a function of mean mantle temperature T . Upon assuming a mean present day temperature of 220 K inside Titan (Stevenson 1992), we find tidally effective material dissipation factors Q_μ in the range 30–50. Provided the core material underwent almost complete dehydration over Titan's thermal history, we can safely neglect tidal heating in the rocky core simply for the reason of too high a silicate viscosity that must be expected for the 220 K present day temperature of Titan's interior, causing the core to respond to tidal distortion almost purely elastically.

As a rough guide for the effective viscosity of the ice–silicate mixture assumed in uniform model **A** we adopt the concept of relative viscosity by replacing Eq. (13) with (Friedson and Stevenson 1983)

$$\nu_{\text{mix}} = (1 - \Phi_{\text{rock}})^{-5/2} \nu_{\text{ice}} \quad (14)$$

to account for the suspension effect leading to greater viscosities in the presence of rock particles in a water-ice matrix. Upon relating the rock particle volume concentration Φ_{rock} to Titan's mean density $\bar{\rho}$ and ice mass fraction f_{ice} according to

$$\Phi_{\text{rock}} = (1 - f_{\text{ice}}) \frac{\bar{\rho}}{\rho_{\text{rock}}} \quad (15)$$

and using $\rho_{\text{rock}} = 3500 \text{ kg m}^{-3}$, we find a relative enhancement in viscosity by a factor of 2.5 with respect to that of pure ice which in turn corresponds to a Newtonian viscosity of order 10^{17} Pa sec at $T = 220 \text{ K}$. Taking

TABLE II
Physical Properties of Titan Materials as Referred to 220 K and $4.56 \times 10^{-6} \text{ s}^{-1}$

	ρ (kg m ⁻³)	μ (GPa)	ν (m ² s ⁻¹)	Q_μ
Ice I	930	3.5	2.42×10^{13}	29.3
NH ₃ –H ₂ O	950	Liquid	Liquid	∞
Ice II	1180	3.5	2.42×10^{13}	37.2
Ice V	1280	3.5	2.42×10^{13}	40.4
Ice VI	1430	3.5	2.42×10^{13}	45.1
Rock	2895–3085	65.0	∞	∞

Note. Incompressibility is assumed throughout the interior of Titan.

$\mu_{\text{ice}} = 4 \text{ GPa}$ and $\mu_{\text{rock}} = 65 \text{ GPa}$ as representative values for the rigidity of the ice and rock components at the tidal frequency (Cassen *et al.* 1982), we get a mean rigidity μ_{mix} of approximately 14 GPa after Voigt–Reuss–Hill averaging, and the tidally effective material dissipation factor Q_μ given in Eq. (12) is found to be approximately 35. It should be noted, however, that the Newtonian suspension model for the effective viscosity of the ice–silicate mixture is restricted to ice grain size less than about 1 cm (Friedson and Stevenson 1983).

We will require the complex Love numbers and mass load coefficients for each model. These are obtained by the numerical integration of the linearized field equations describing small viscoelastic deformations in a self-gravitating sphere subject to certain continuity and boundary conditions. Based on the correspondence principle (cf. Zschau 1978) relating the viscoelastic problem to the well-known problem of small elastic deformations, standard Runge–Kutta methods in the frequency domain can be employed to solve for the complex radial factors h_2, h'_2 and k_2, k'_2 of radial displacement and potential perturbation, respectively (Longman 1962, 1963). The h_2 and k_2 mentioned are the Love numbers while h'_2 and k'_2 are the mass load coefficients. Considering the surface boundary conditions, it should be emphasized that the stress field due to body forces acting on a planetary body differs from that due to mass loading of the free surface. In the absence of oceans and seas on Titan and disregarding atmospheric loading effects, the surface would be kept in a stress-free state where the complex Love numbers are referred to as a consequence of vanishing radial and tangential stress components upon body tide forcing. In contrast, tidal loading in the presence of an ocean would result in a nonvanishing radial stress component and special care has to be taken when calculating complex mass load coefficients.

The assumed material properties for our interior models of Titan are shown in Table II. It should be noted that the density difference of the core material for models **B** and **C** is due to the mass balance constraints, namely

TABLE III
Complex Love Numbers and Mass Load Coefficients

	Model A		Model B		Model C	
	\Re	$100 \times \Im$	\Re	$100 \times \Im$	\Re	$100 \times \Im$
h_2	0.1192	-0.3225	0.0587	-0.0796	1.1900	-0.5673
k_2	0.0716	-0.1935	0.0263	-0.0288	0.3590	-0.1711
h_2^i	-0.0795	0.2150	-0.0797	0.1414	-2.7530	1.3130
k_2^i	-0.0477	0.1290	-0.0325	0.0508	-0.8307	0.3961
h_f	2.5000	—	1.9020	—	1.4300	—
k_f	1.5000	—	0.9253	—	0.4304	—

Note. \Re denotes real part and \Im is imaginary part of corresponding complex Love number and mass load coefficient, respectively.

satisfying Titan's surface gravity of 1.35 m sec^{-2} . The core densities inferred in this way are well in accordance with typical densities of rock materials ranging from about 2500 kg m^{-3} for hydrated silicates up to 3500 kg m^{-3} for anhydrous silicate and iron (Schubert *et al.* 1986).

The resulting Love numbers for the three models are shown in Table III. Therein, the fluid Love numbers h_f and k_f pertaining to the completely relaxed equilibrium configuration may be interpreted as a measure for the concentration of mass toward the center of Titan (Zharkov *et al.* 1985).

DISSIPATION IN THE INTERIOR DUE TO BODY AND LOADING TIDES

According to the first law of thermodynamics, the rate at which energy is dissipated in Titan's interior by tidal forcing is given by

$$\frac{dE}{dt} = \frac{dE_V}{dt} + \frac{dE_S}{dt} = \int_V \left\langle \rho_0 \frac{\partial \vec{u}}{\partial t} \cdot \nabla \Phi_2 \right\rangle dV + \int_S \left\langle \frac{\partial \vec{u}}{\partial t} \cdot \vec{\tau} \right\rangle dS, \quad (16)$$

where $\langle \dots \rangle$ indicates averaging the work function over one orbital period. The rate dE_V/dt at which work is done by body forces is represented by the volume integral while the surface integral delineates the rate dE_S/dt at which work is done by surface tractions (Love 1927, Zschau 1978). Here ρ_0 denotes unperturbed density, \vec{u} is the displacement vector, $\vec{\tau}_s$ is the surface traction, and the total tidal potential Φ_2 results from the superposition

$$\Phi_2 = \Phi_2^\xi + \Phi_2^i \quad (17)$$

of the primary external tidal disturbance potential Φ_2^ξ and the secondary internal disturbance potential Φ_2^i as induced

by the internal redistribution of mass upon tidal deformation of Titan's interior. Note that the integrations in Eq. (16) refer to the unstrained state of Titan (Zschau 1978, Platzman 1984). Moreover, Titan's comparatively long tidal period of 15.945 days suggests that both the body and loading tides can be best represented by an equilibrium theory. In the case of the body tide, the surface integral in Eq. (16) completely vanishes since either the tangential tractions or the time-averaged product $\langle \partial u_r / \partial t \tau_r \rangle$ of the normal components will be zero (Zschau 1978). On the other hand, the latter will be significant in the case of loading tides provided that the surface of Titan is covered by satellite-wide seas and oceans and does not go to zero in any case since there would still be the much smaller atmospheric load. With the aid of Green's first integral transformation and using some knowledge of the potentials, the volume integral in Eq. (16) simplifies to the surface integral

$$\frac{dE_V}{dt} = -\frac{5}{4\pi GR_T} \int_S \langle \Phi_2^i \dot{\Phi}_2^\xi \rangle dS \quad (18)$$

to be taken over Titan's surface having radius R_T (Zschau 1978, Segatz *et al.* 1988). The dot over Φ_2^i indicates derivation with respect to time.

The inelastic response of Titan's interior to body tides is assumed to give rise to the dissipation of tidal energy. Given that the tidally induced deformation of Titan's surface is small, this can be expressed in terms of the second-order complex Love number $k_2 = \Re(k_2) + i\Im(k_2)$ according to the proportionality

$$\Phi_2^i = k_2 \cdot \Phi_2^\xi \quad (19)$$

between secondary and primary disturbance potential.

Upon inserting Eq. (19) into Eq. (18) and taking advantage of the fact that $|\Im(k_2)| \ll |\Re(k_2)|$ generally holds true for planetary interiors, we arrive at

$$\frac{dE}{dt} = -\frac{5}{4\pi GR_T} \Re(k_2) \int_S \langle \Phi_2^\xi \dot{\Phi}_2^\xi \rangle dS, \quad (20)$$

where the bullet mark indicates the small phase lag angle $\delta_2^i = \Im(k_2)/\Re(k_2)$ of the secondary potential Φ_2^i relative to the primary external tidal disturbance potential Φ_2^ξ (Zschau 1978). Substituting the expression for Φ_2^ξ as given in Eq. (6) into Eq. (20) and using Eq. (19) yields the global tidal dissipation rate due to the body tide (Segatz *et al.* 1988)

$$\frac{dE}{dt} = -\frac{21}{2} \Re(k_2) \frac{(nR_T)^5}{G} e^2 \quad (21)$$

as a function of the imaginary part of the complex love number k_2 that depends on the rheological behavior of Titan's solid parts as well as on the interior structure of Titan as a whole. This is the same as is commonly given (cf. Peale 1986) if the approximation $\Im(k_2) = -\Re(k_2)/Q$ is used. Note that $\Im(k_2)$ and all phase lags are negative in our notation and that we use the convention of a positive dE/dt as indicating energy loss.

In order to obtain the global tidal dissipation rate as a consequence of loading tides due to a putative global ocean on Titan, we will follow a method apparently first outlined by Zschau (1978). To start with, we must replace the expression for the primary external disturbance potential in Eq. (6) by the potential due to the attraction of the ocean tide

$$\Phi^p = 4\pi GR_T \sum_{l=2}^{\infty} \left(\frac{R_T}{R}\right)^{l+1} \frac{\sigma \xi_l}{2l+1} \quad (22)$$

where σ is ocean density and ξ_l is relative height of the ocean tide of harmonic degree l (Kaula 1968). As mentioned earlier, the largest contribution to the external tidal disturbance is expected to arise from Φ_2^e . Accordingly, we may approximate Eq. (22) to first order on Titan's surface and get

$$\Phi^p \approx \Phi_2^e = \frac{4\pi GR_T}{5} \sigma \xi_2 \quad (23)$$

with

$$\xi_2 = \gamma_2 \cdot \frac{\Phi_2^e}{g_s}, \quad (24)$$

where the real parts of the complex Love numbers k_2 and h_2 enter the correction factor $\gamma_2 = 1 + \Re(k_2) - \Re(h_2)$ that accounts for Titan's elastic response and upward displacement of the ocean bottom. When the surface gravity is taken as

$$g_s = \frac{4}{3} \pi G \bar{\rho} R_T, \quad (25)$$

then Eq. (23) reduces to

$$\Phi_2^p = \frac{3}{5} \gamma_2 \frac{\sigma}{\bar{\rho}} \Phi_2^e, \quad (26)$$

where $\bar{\rho}$ is Titan's mean density.

The inelastic response of Titan's interior to the tidally induced variable ocean load results in an additional radial displacement of the ocean bottom of

$$u_r = h_2' \cdot \frac{\Phi_2^e}{g_s}, \quad (27)$$

which lags behind the external tidal disturbance potential Φ_2^e by $\delta_2^* = \Im(h_2')/\Re(h_2')$. In analogy to Eq. (19), this gives rise to a secondary disturbance potential

$$\Phi_2^s = k_2' \cdot \Phi_2^e \quad (28)$$

having a different phase lag $\delta_2^i = \Im(k_2')/\Re(k_2')$ relative to Φ_2^e . The complex quantities h_2' and k_2' are referred to as the complex mass load coefficients (Zschau 1978). When replacing the volume integral in Eq. (16) by a surface integral as was done in Eq. (20) and substituting the normal traction

$$\tau_r = -(\sigma \xi_2 + \rho_0 u_r) g_s \quad (29)$$

in the surface integral in Eq. (16), we get

$$\frac{dE}{dt} = \frac{5}{4\pi GR_T} \left(\frac{3}{5} \gamma_2 \frac{\sigma}{\bar{\rho}}\right)^2 \left[\Re(h_2') \int_S \langle \Phi_2^{e*} \Phi_2^e \rangle dS - \Re(k_2') \int_S \langle \Phi_2^{e*} \Phi_2^s \rangle dS \right] \quad (30)$$

by applying Eq. (25) to Eq. (29) and rearranging. Note that the different markings indicate the difference in phase angles δ_2^* and δ_2^i relative to Φ_2^e as mentioned before. Upon insertion of Φ_2^s as given in Eq. (6), we then get the global dissipation rate due to the loading tide

$$\frac{dE}{dt} = \frac{21}{2} (\Im(h_2') - \Im(k_2')) \frac{(nR_T)^5}{G} e^2 \left(\frac{3}{5} \gamma_2 \frac{\sigma}{\bar{\rho}}\right)^2 \quad (31)$$

with the complex mass load coefficients h_2' and k_2' parameterizing the constitution of Titan's deep interior.

OCEAN TIDAL DISSIPATION

Sagan and Dermott (1982) performed their calculations for a pure methane ocean ($\sigma = 450 \text{ kg m}^{-3}$), whereas it is now known that a pure methane ocean is not compatible with Voyager I radio-occultation and IRIS data. For reasonable bounds on ocean composition see Dubouloz *et al.* (1989), although the concept of an ethane-rich ocean is due to Lunine *et al.* (1983). The depth estimates of Lunine *et al.* (1983) and Dubouloz *et al.* (1984) were based on an early photochemical model (Yung *et al.* 1984) which predicted a 600-m accumulation of ethane on the surface over the age of the Solar System, giving a range of allowable ocean depth D of 700 m (ethane-rich) to 9 km (methane-rich) (Dubouloz *et al.* 1989). However, improved pho-

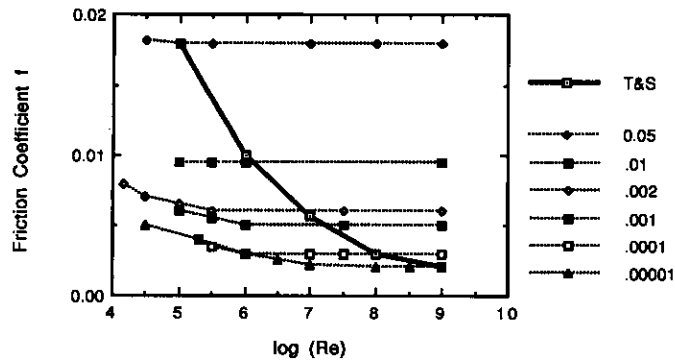


FIG. 4. Friction coefficient f_b as a function of bottom roughness and Reynolds number. Dotted curves are data from Massey (1979) for various values of bottom roughness (roughness scale divided by ocean depth) and may be compared with the expression in Eq. (32) due to Turcotte and Schubert (1982).

tochemical models, giving better agreement with observational data, have become available and suggest a pure-ethane depth of order 250 m corresponding to a maximum ocean depth of order 5 km (Lara 1993, Lara *et al.* 1994).

The question of the friction coefficient f_b is also nontrivial. Sagan and Dermott (1982) use $f_b = 0.002$, as do many other workers on oceans. This value can be traced back to original work with water by Jeffreys (1925). However, we now know that f_b is a function of surface roughness and the Reynolds number of the flow. Massey (1979) gives f_b in graphical form as a function of Reynolds' number and bottom roughness in his Fig. 7.2. An empirical expression for f_b is given by Turcotte and Schubert (1982) as

$$f_b = 0.3164Re^{-1/4}. \quad (32)$$

See Fig. 4. The Reynolds number is

$$Re = \sigma vl/\eta, \quad (33)$$

where the length scale l is normally taken to be the depth D . For a typical terrestrial ocean ($v = 1 \text{ m sec}^{-1}$, $\sigma = 1000 \text{ kg m}^{-3}$, $D = 1000 \text{ m}$, $\eta = 10^{-3} \text{ Pa sec}$) Re is of order 10^9 , leading to $f_b \approx 0.002$. For Titan, the tidal velocities are lower and the density is lower. For a rough guide of the Reynolds number, we use $v = 0.1 \text{ m sec}^{-1}$ and a density of 650 kg m^{-3} . The viscosity of non-polar hydrocarbons is typically $6 \times 10^{-4} \text{ Pa sec}$, giving $Re = 10^8$ and $f_b \approx 0.003$, though see the discussion around Eq. (51).

Previous work has assumed a composition of liquid methane to evaluate tidal dissipation, with a density value $\sigma = 450 \text{ kg m}^{-3}$, and we have used this value in selected cases to compare results. However, as mentioned above the possible composition can vary from ethane-rich to

methane-rich (Dubouloz *et al.* 1989). While it might be expected that an ethane-rich ocean would be more dense than a methane-rich one since the density of ethane is about 650 kg m^{-3} , it turns out that the increased solubility of atmospheric nitrogen (density of liquid nitrogen $\approx 720 \text{ kg m}^{-3}$) in a methane-rich ocean largely compensates for the less dense methane. Lorenz (1992b) calculated the density of the two extreme cases in Dubouloz *et al.* (1989) and found them to be 605 and 645 kg m^{-3} . Since these computations ignore propane, a liquid under Titan surface conditions, other organic solutes, and suspended solid particles, our "nominal" ocean has a density of 650 kg m^{-3} and is referred to as model **a**.

In principle, it could be possible for an ocean to have a density below 650 kg m^{-3} , if it had large quantities of gas bubbles suspended in it. However, we do not consider this exotic case, since it requires special circumstances to maintain a bubble population, and the resultant density does not lead to extreme dissipation. Nevertheless, as mentioned above we do consider a pure methane ocean with a density of 450 kg m^{-3} , for comparison with Sagan and Dermott (1982). This is referred to as model **b**.

As a limiting case, we also consider a shallow, sludge ocean since according to Lara *et al.* (1994) the deposition rates of ethane and propane, the liquid photochemical products, are comparable with the deposition rate of impact ejecta and solid products. Thus $D = 300 \text{ m}$, $\sigma = 800 \text{ kg m}^{-3}$, and $\eta \approx 1 \text{ Pa sec}$ (the value for heavy crude oil on Earth) gives $Re = 2.4 \times 10^4$ and hence $f_b \approx 0.02$. We take a density of 800 kg m^{-3} for our viscous "sludge" ocean model **c** since it is intermediate between the value of ice and ocean.

Analytic Model of Dissipation Due to Bottom Friction

In the case of a global ocean covering the surface of Titan, the energy loss is believed to be caused by bottom frictional dissipation according to

$$\frac{dE}{dt} = f_b \sigma \int_S \langle (u^2 + v^2)^{3/2} \rangle dS, \quad (34)$$

where $\langle \dots \rangle$ indicates averaging over one orbital period and $(u^2 + v^2)^{1/2}$ is the vertically averaged flow speed of the tidal ocean currents. Provided the work done by these currents on the sea bottom equals the work Saturn does on the surface of Titan's sea, Eq. (34) can be replaced by (Lambeck 1978, Zahel 1980)

$$\frac{dE}{dt} = -\sigma \gamma_2 \int_S \langle \Phi_2^{\diamond} \dot{\xi}_2 \rangle dS \quad (35)$$

or, upon inserting Eq. (24), the relative height of the ocean tide,

$$\frac{dE}{dt} = -\frac{\sigma}{g_s} \gamma_2^2 \int_S \langle \Phi_2^{\diamond} \dot{\Phi}_2^{\diamond} \rangle dS, \quad (36)$$

where the diamond mark indicates that there will be a small phase lag δ_2^{\diamond} of the tidal wave relative to the primary disturbance potential Φ_2^{\diamond} . In this approximation, tidal loading and ocean self-attraction are neglected. Since we may limit ourselves here to the case of bottom friction dissipation, we can relate such a phase lag to the tidally effective specific dissipation function Q_b of the ocean current:

$$\sin \delta_2^{\diamond} \approx \tan \delta_2^{\diamond} = -Q_b^{-1}. \quad (37)$$

Upon inserting Eq. (6) for Φ_2^{\diamond} in Eq. (36), integrating over the sea surface of Titan, and taking advantage of Eq. (37), one may end up with the global dissipation rate

$$\frac{dE}{dt} = \frac{21}{2} \frac{(nR_T)^5}{G} e^2 \frac{1}{Q_b} \left(\frac{3}{5} \gamma_2^2 \frac{\sigma}{\rho} \right) \quad (38)$$

due to bottom friction losses of the ocean tide. Note that this is the same as Eq. (21) with

$$\frac{1}{Q_b} \left(\frac{3}{5} \gamma_2^2 \frac{\sigma}{\rho} \right) \Leftrightarrow -\Im(k_2) \approx \frac{\Re(k_2)}{Q}, \quad (39)$$

thus giving us a way to generate dissipation rates based on an oceanic quality factor. Even though we are restricting ourselves here to bottom friction, Eq. (38) is more general, though it does assume synchronous rotation.

Next, we apply the analytical model apparently first presented by Goldreich and Soter (1966) to obtain the quality factor Q_b in Eq. (38). When the general definition for the quality factor is taken as

$$Q_b = 2\pi \frac{E_0}{\Delta E} \quad (40)$$

with

$$E_0 = \frac{1}{2} \sigma g_s \xi_2^2 \quad (41)$$

as the maximum potential energy per unit area stored in the tidal wave of maximum relative height ξ_2 and

$$\Delta E = \frac{2\pi}{n} R_b \quad (42)$$

as the energy dissipated over one tidal cycle where (Munk and MacDonald 1989)

$$R_b = f_b \sigma \bar{v}_b^3 \quad (43)$$

is the energy dissipation rate per unit area, then

$$Q_b = \frac{1}{2} \frac{n g_s \xi_2^2}{f_b \bar{v}_b^3} \quad (44)$$

is inferred as a reasonable estimate for the quality factor of an ocean current moving across the surface of Titan. The average background ocean current velocity \bar{v}_b is given by

$$\bar{v}_b = \frac{1}{2} (nR_T) \frac{\langle \xi_2 \rangle}{D} \quad (45)$$

with D as ocean depth and

$$\langle \xi_2 \rangle = \gamma_2 \frac{\langle \Phi_2^{\diamond} \rangle}{g_s} \quad (46)$$

as relative height of the corresponding tidal wave as averaged over time. As usual, we may replace ξ_2 with

$$\xi_2 = \gamma_2 \frac{\hat{\Phi}_2^{\diamond}}{g_s} \quad (47)$$

Furthermore, we may recall here that Φ_2^{\diamond} as the primary tidal disturbance potential varies periodically between $1.5 (nR_T)^2 e$ and $3.2 (nR_T)^2 e$ (Segatz *et al.* 1988), so that

$$\xi_2 = 3.2 \gamma_2 \frac{(nR_T)^2 e}{g_s} \quad (48)$$

and using Eq. (7) to find the size of the primary bulge, with a correction of $2/\pi$ to allow for the sinusoidal shape, results in

$$\langle \xi_2 \rangle = 1.7 \gamma_2 \frac{(nR_T)^2 e}{g_s} \quad (49)$$

Upon replacing g_s as given in Eq. (25), we finally get from Eq. (44)

$$Q_b = \frac{4^3 \times 3.2^2}{3^2 \times 1.7^3} \pi^2 \frac{(\bar{\rho}G)^2}{f_b \gamma_2 e n^4} \left(\frac{D}{R_T} \right)^3 = 14.8 \pi^2 \frac{(\bar{\rho}G)^2}{f_b \gamma_2 e n^4} \left(\frac{D}{R_T} \right)^3 \quad (50)$$

as quality factor for an ocean current on a synchronously rotating satellite. It should be noted that Eq. (45) allows us to dimension the Reynolds number of the tidal flow given in Eq. (33) according to

$$Re \approx 0.2\gamma_2 \frac{n^3 R_T^2 e \sigma}{\eta G \bar{\rho}} \quad (51)$$

and hence to infer f_b self-consistently by using the empiric expression given in Eq. (32). For the nominal ocean and $\eta = 6 \times 10^{-4}$ Pa sec, this translates to $Re \approx \gamma_2 \times 10^7$, and since γ_2 is 0.96, 0.97, and 0.16 for models **A**, **B**, and **C**, respectively, our earlier estimate of $Re \approx 10^8$ was too high, probably because of an overestimate of the flow velocity.

This lower Re leads to a somewhat larger f_b than has been used for the nominal ocean. For the Re above, Eq. (32) gives an f_b of 0.0056 for models **A** and **B** and 0.009 for **C**. However, Fig. 4 shows that there can be considerable variation in f_b . Therefore, while Eq. (32) is convenient, it must be used with care. In any case, the f_b corresponding to the Re computed above is lower than that for a sludge ocean; thus our nominal and sludge oceans still represent useful bounds on ocean dissipation.

Other Ocean Models

Sagan and Dermott (1982) also published an analytical model for the fluid dissipation in Titan. Using only the radial portion of the tide, they estimated the dissipation to be

$$\frac{dE}{dt} = 216f_b\sigma(hne)^2 \frac{R_T^5}{105\pi D^3}, \quad (52)$$

where h here is the equilibrium tide height, which they took to be 100 m. Using $f_b = 0.003$ and $\sigma = 650 \text{ kg m}^{-3}$, this reduces to (Sears 1994)

$$\frac{dE}{dt} = 3.4 \times 10^{17}/D^3. \quad (53)$$

Note that Sagan and Dermott (1982) used $f_b = 0.002$ and $\sigma = 450 \text{ kg m}^{-3}$ and therefore produced correspondingly smaller dissipations. Also, since they left out the effects of the libration and coriolis forces, this is a lower limit for any set of parameters.

One of us has produced a numerical model of the ocean tidal dissipation (Sears 1995). This model uses a 2° under-sampled grid and the vertically integrated hydrodynamic fluid equations and is modeled on the Earth-ocean tidal models of Zahel (1970, 1973, 1977, 1978, 1980). Please see Sears (1995) for details. An approximation to the numerical results in the form of Eq. (53) was also produced:

$$\frac{dE}{dt} = 2 \times 10^{18}/D^3 \quad (54)$$

and is accurate to one significant figure over a limited

range. Note that his model assumes that Titan has not hydrostatically relaxed, whereas our use of the potential in Eq. (6) implicitly assumes relaxation.

RESULTANT TIDAL DISSIPATION RATES

Figure 5 illustrates for each of the interior models **A**, **B**, **C** how the ocean tidal dissipation rate and its corresponding contribution to the steady-state surface heat flow depend on depth and composition of Titan's putative global ocean. For comparison, the background dissipation rates due to body and loading tides are shown as well. It is evident that dissipation due to ocean loading is of minor importance, generally, when compared to the body tide background which proves to be between one and two orders of magnitude higher. The largest solid dissipation rate is clearly produced for the differentiated volatile-rich model **C** owing to the greater flexibility of its 150 km thick outer Ice I shell mechanically decoupled from the deep interior through the internal $\text{NH}_3\text{-H}_2\text{O}$ ocean and therefore subject to larger tidal strain rates. Recalling, however, that the homogeneous ice/rock model **A** permits tidal heating throughout the whole interior, it is capable of obtaining higher solid dissipation rates than the differentiated volatile-poor model **B** for which, in contrast, dissipation of tidal energy is neglected in the 1900-km radius rocky core. Otherwise, models **A** and **B** produce similar ocean dissipation rates simply because both have similar correction factors γ_2 entering into the dissipation formula via Eqs. (38) and (50). For both models, γ_2 is not too different from that of the rigid body equivalent $\gamma_{\text{rigid}} = 1$, indicating zero displacement of the ocean bottom upon tidal forcing. In contrast, model **C** produces much lower ocean dissipation rates due to an extremely small value of $\gamma_2 = 0.16$, resulting in greater motion of the ocean floor and thus giving smaller ocean currents. It is, however, interesting to note that it is that same higher flexibility of model **C** which causes the solid dissipation larger than that of model **B**. The amount of solid dissipation in the outermost ice shell is supposed to be limited by the shell volume itself and is comparable to the whole-interior dissipation of model **A**.

Furthermore, it becomes obvious from examination of Fig. 5 that the precise density of a global ocean made of nonpolar hydrocarbons may vary between that of methane-rich (ocean model **a**) and the nominal ethane-rich (ocean model **b**) compositions without having any pronounced effect on the resultant dissipation due to bottom friction. Note, however, that the dissipation rates in the case of a more viscous and more dense sludge ocean (ocean model **c**) prove to be an order of magnitude higher. The dissipation in the solid portion of Titan due to body and loading tides is shown in Table IV along with the dissipation for the nominal ocean **b** of various depths.

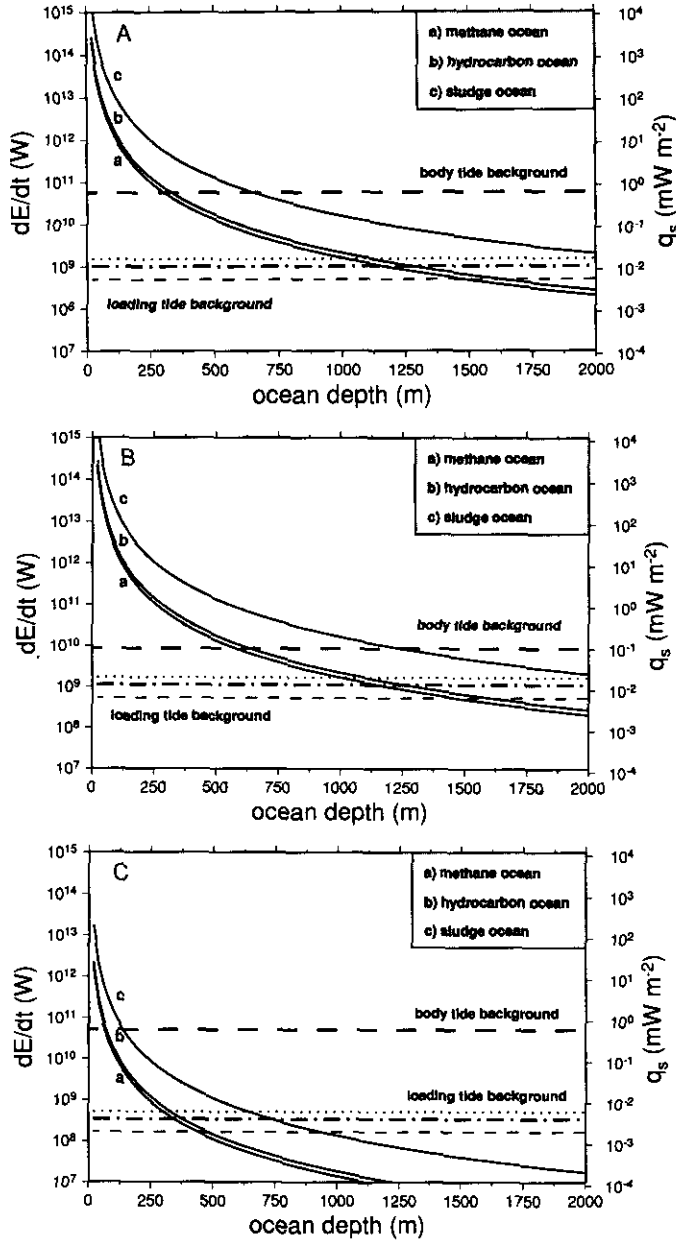


FIG. 5. Tidal dissipation rate dE/dt and corresponding surface heat flow q_s as a function of ocean depth for interior models A, B, and C. The horizontal lines show the solid body dissipation for comparison. The loading tide depends on the ocean density. The dash-dot lines are for the nominal ocean, the dashed lines are the methane ocean, and the dotted lines are the sludge ocean.

Note the inclusion of the atmospheric loading tide for the zero-depth ocean case.

Table V shows the nominal ocean dissipation rates as a function of depth for each interior model compared to the results of the numeric model of Sears (1995) and the analytic model of Sagan and Dermott (1982) according to Eq. (53). Note, however, that both authors assumed interior structures of water ice but with a density of 1881 kg m^{-3} . This makes them most compara-

TABLE IV
Dissipation Rates for the Various Titan Models and the Nominal Ocean

Depth(m)	Tidal dissipation rates (W)			Total dissipation
	Body dissipation	Load dissipation	Ocean dissipation	
Model A ($f_b = 0.0042$)				
0	5.8×10^{10}	6.9×10^4	—	5.8×10^{10}
100	5.8×10^{10}	1.0×10^9	2.1×10^{12}	2.2×10^{12}
400	5.8×10^{10}	1.0×10^9	3.3×10^{10}	9.2×10^{10}
600	5.8×10^{10}	1.0×10^9	9.8×10^9	6.9×10^{10}
1000	5.8×10^{10}	1.0×10^9	2.1×10^9	6.1×10^{10}
Model B ($f_b = 0.0042$)				
0	8.6×10^9	7.5×10^4	—	8.6×10^9
100	8.6×10^9	1.1×10^9	2.2×10^{12}	2.2×10^{12}
400	8.6×10^9	1.1×10^9	3.5×10^{10}	4.4×10^{10}
600	8.6×10^9	1.1×10^9	1.0×10^{10}	2.0×10^{10}
1000	8.6×10^9	1.1×10^9	2.2×10^9	1.2×10^{10}
Model C ($f_b = 0.0065$)				
0	5.1×10^{10}	2.3×10^4	—	5.1×10^{10}
100	5.1×10^{10}	3.4×10^8	1.8×10^{10}	7.0×10^{10}
400	5.1×10^{10}	3.4×10^8	2.9×10^8	5.2×10^{10}
600	5.1×10^{10}	3.4×10^8	8.5×10^7	5.2×10^{10}
1000	5.1×10^{10}	3.4×10^8	1.8×10^7	5.2×10^{10}

Note. The loading dissipation for the zero-depth ocean is due to the atmosphere. f_b denotes bottom friction coefficient.

ble with interior model A of the present study. The Sagan and Dermott formulation produces values which are about one-sixth of our model, while the numeric model results are within about 20% of our model. The low estimate of the Sagan and Dermott formulation is probably due to only using the radial tide, which Sears (1995) indicates is responsible for only about one-fifth of the total dissipation. The differences between our model and the numeric model seem to be primarily due to the fact that the numeric model indicates that the

TABLE V
Comparison of Tidal Models

Depth (m)	Model				
	A (W)	B (W)	C (W)	S&D (W)	Numeric (W)
100	2.1×10^{12}	2.2×10^{12}	1.8×10^{10}	3.5×10^{11}	2.5×10^{12}
400	3.3×10^{10}	3.5×10^{10}	2.9×10^8	5.3×10^9	3.2×10^{10}
600	9.8×10^9	1.0×10^{10}	8.5×10^7	1.6×10^9	8.8×10^9
1000	2.1×10^9	2.2×10^9	1.8×10^7	3.5×10^8	1.7×10^9

Note. S&D is the Sagan and Dermott (1982) model as shown in Eq. (53). Note that several of the parameters are different between the three models of this paper and the S&D and numeric models.

dependency is slightly stronger than inverse depth to the third power. Also, both of these alternative models assume a spherical Titan while here we assume a hydrostatically relaxed prolate Titan.

DECAY OF ORBITAL ECCENTRICITY

The tidal dissipation represents a loss of Titan's orbital energy about Saturn since the only source of energy is the orbit, assuming synchronous rotation. This manifests itself primarily as a reduction in orbital eccentricity and a much slower change in semimajor axis (Sears 1995). Thus Titan's current eccentricity of 0.0292 provides a clue to its past.

The change in eccentricity due to tidal energy dissipation is

$$\frac{de}{dt} \frac{e}{1-e^2} = \frac{-a}{GM_S M_T} \frac{dE}{dt} \quad (55)$$

where M_S is the mass of Saturn and M_T is the mass of Titan, and $\dot{E} > 0$ indicates an energy loss.

The solid body dissipations have an e^2 dependency and the ocean dissipation has an additional e dependency hidden in the Q_b formula (Eq. 50). For the e^2 dependency case, and taking into account the relationship between a and e implied by conservation of angular momentum ($a(1-e^2) = \text{const.}$), integrating Eq. (55) gives

$$e' = e_0 \exp\left(\frac{a_0(1-e_0^2)}{GM_S M_T e_0^2} \frac{dE}{dt} t\right), \quad (56)$$

where t is time into the past, the prime mark indicates values at that time, and the zero subscript indicates current values (Sears 1995). Upon taking $e'/e = \exp(1)$, i.e., restricting e' to be less than 0.08, and using Kepler's third law $GM_S = n^2 a^3$, we get the current e -folding time for the decay of the orbital eccentricity τ_{decay} for small eccentricity values:

$$\tau_{\text{decay}}^{\text{solid}} = \frac{(ane)^2 M_T}{1-e^2} \left(\frac{dE}{dt}\right)^{-1} \approx (ane)^2 M_T \left(\frac{dE}{dt}\right)^{-1}. \quad (57)$$

The secular acceleration \dot{n}/n is related to τ_{decay} simply by

$$\frac{\dot{n}}{n} = \frac{3\dot{E}}{2E} = \frac{3e^2}{\tau_{\text{decay}}}. \quad (58)$$

Note that these formulas are not strictly correct for the $\dot{E} = ce^3$ dependency of the ocean models, wherein the

constant of proportionality, c , may be easily derived by comparing with Eqs. (38) and (50). As noted earlier by Sagan and Dermott (1982) the time scale for the decay of orbital eccentricity in the e^3 dependency case can be written in the form

$$\tau_{\text{decay}}^{\text{ocean}} = \frac{E}{ce}, \quad (59)$$

where

$$E = \frac{1}{2} \frac{GM_S M_T}{a}$$

is total orbital energy of Titan. Accordingly, the secular acceleration then becomes

$$\frac{\dot{n}}{n} = \frac{3}{2} \frac{e^2}{\tau_{\text{decay}}}, \quad (60)$$

implying to be half of that given in the e^2 dependency case above.

For each of the interior models **A**, **B**, and **C**, Fig. 6 gives the time constant for decay of orbital eccentricity along with Titan's secular acceleration versus ocean depth. As in Fig. 5, the background contribution due to body and loading tides is shown for comparison. It is obvious that the solid dissipation rates as provided by the homogeneous interior model **A** and the differentiated volatile-rich model **C** are too high to permit preserving Titan's orbital eccentricity over the age of the Solar System, which we take as 4.55 aeons. (1 aeon = 10^9 years.) The two models **A** and **C** require a time constant of orbit circularization close to 2 aeons as a consequence of comparably high solid background dissipation through body tides. Using such interior structure models, therefore, would make Titan's current orbital eccentricity hard to understand. The possibility has been noted before, such as when Peale *et al.* (1980) wrote "Even Titan, although a marginal case, would have had its eccentricity damped below its present value of 0.0289 for reasonable values of original eccentricity. . . ."

It is tempting to claim that we can now restrict ourselves to the differentiated volatile-poor model **B** as the one model which meets with the known dynamic constraints in that the orbit circularization time scale is about 13 aeons in the absence of an ocean. Equations (57) and (59) show that τ_{decay} is proportional to the inverse dissipation rate. Since the dissipation associated with the interior is present regardless of the ocean, and the two dissipations are additive, this gives us a restriction on the dissipation and associated τ_{decay} of the ocean, and hence on the mini-

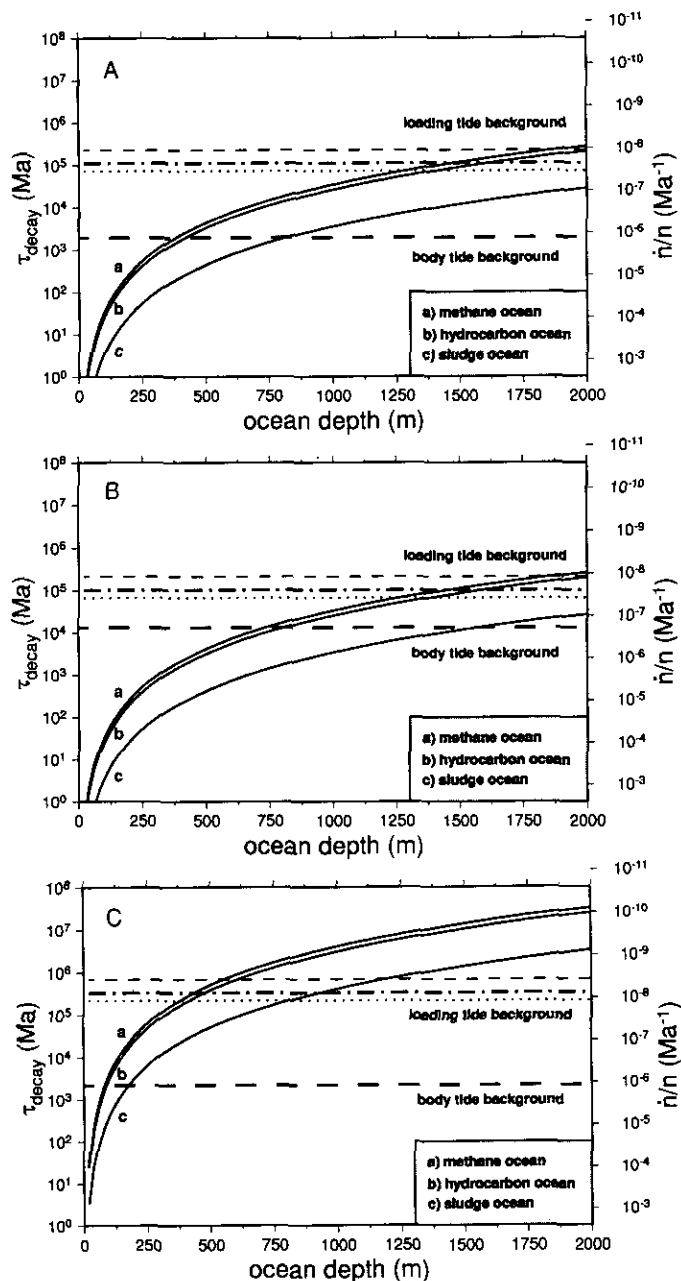


FIG. 6. Orbital $1/e$ decay timescale τ_{decay} and corresponding secular acceleration \dot{n}/n as a function of ocean depth for interior models A, B, and C. Note, however, that the secular acceleration ordinate refers to the e^2 dependence used for Eq. (56), thereby overestimating the true e^3 dependence of the ocean models by a factor of 2. The horizontal lines show the eccentricity lifetime due to the solid body dissipation for comparison. As in Fig. 5 the loading tide depends on the ocean density. The dash-dot lines are for the nominal ocean, the dashed lines are for the methane ocean, and the dotted lines are for the sludge ocean.

imum ocean depth, as always assuming its existence and global coverage of Titan's surface. For an interior τ_{decay} of 13 aeons, the associated minimum time scale for an ocean must be 7 aeons. Examination of the middle portion

of Fig. 6 indicates that such an ocean must be deeper than 560 m for the nominal ocean model **b** in order to let the total time constant of orbital decay be comparable to or larger than the age of the Solar System. This minimum depth is reached at 510 m even in the case of a pure methane ocean (ocean model **a**) as proposed by Sagan and Dermott (1982). A more viscous sludge ocean (ocean model **c**) deeper than 1100 m would be also in accordance with the dynamic constraints.

Perhaps more plausible than a deep sludge ocean, however, is a deep regolith layer, with the liquid ethane/methane stored in pores, channels, and caverns beneath the surface. As noted by Stevenson (1992), such a surface model satisfies observational constraints, and the dissipation would be low since the fluid would be unable to respond as quickly to the tidal potential, and hence would have a much lower velocity. While the distinction between a sludge ocean and a buried ocean may be somewhat arbitrary, the endmember cases of these two possibilities are radically different. A "thin" sludge is just a silty ocean and increasing the solid content increases the viscosity and the dissipation while slowly decreasing the flow velocity. However, a very thick sludge, or a "buried ocean," would have a flow so small that even the extremely high friction coefficient would not produce a large dissipation.

The approach here is necessarily limited, since in Titan's distant past, each of its orbital parameters, not only the eccentricity, may have been significantly different, and the interior will most likely have had a different structure. The delivery of methane and ethane to form reservoirs on the surface may not have been instantaneous at the "beginning of the Solar System." The history of the surface volatile inventory may have a significant effect on the tidal dissipation over the age of the Solar System. Further, about 3 aeons ago, much of the atmosphere and ocean may have been frozen on the surface (McKay *et al.* 1993). In a frozen state it would have had a much lower dissipation.

ORIGIN OF TITAN'S ECCENTRICITY

The expected high dissipation in both the interior and in any oceans on the surface complicates our understanding of Titan's eccentricity. While there are some models which are consistent with the eccentricity being primordial, models which are acceptable in other respects are inconsistent with this assumption. Thus we explore here mechanisms for the recent generation or maintenance of the eccentricity.

No saturnian satellites large enough or near enough to Titan have been observed which could maintain eccentricity against dissipation (as occurs for Io in the jovian system, for example). The only remote possibility is perhaps

the progenitor of Hyperion. Hyperion, an irregular satellite, now in a 4:3 resonance orbit with Titan, is believed to be the remnant of a much larger (spherical) body that was disrupted by a catastrophic collision (Smith *et al.* 1982). However, it seems fruitless to explore whether such a body, which might have had a radius as large as 1000 km, could have maintained Titan's eccentricity by orbital resonance, since over 90% of the fragments of proto-Hyperion's disruption would have impacted Titan within 100 years (Farinella *et al.* 1990). These impacts themselves would have modified the eccentricity. Further, a high free eccentricity for Titan being due to a recent capture of Titan by Saturn seems implausible, since such a capture would presumably have disrupted the orbits of other satellites extensively.

Thus, we are left with only two obvious possibilities for generating a significant orbital eccentricity for a Titan with an initially circular orbit: impact or close encounter with one or more large bodies, either saturnocentric or interplanetary. Stevenson (1992) has noted that an impact origin of the eccentricity would require an object the size of one of the other saturnian satellites. In this section, we examine more explicitly the kind of object required.

It can be shown that to generate an orbit with an eccentricity e from an initially circular orbit requires a velocity change ΔV of

$$\Delta V = \sqrt{\frac{GM_S}{a}}(\sqrt{1+e} - 1). \quad (61)$$

For the parameters in Table I, the current Titan requires a ΔV of order 80 m sec^{-1} . However, remember that the further in the past the encounter occurred, the larger ΔV required since Titan would have been dissipating energy ever since.

A ΔV of 80 m sec^{-1} requires an impulse (multiplying by Titan's mass) of order 10^{25} N sec . For a Saturn-Neptune planetesimal, with an arrival velocity of 10 km sec^{-1} , this corresponds to a mass of at least 10^{21} kg (i.e., about 1000 km in diameter for a density of about 2000 kg m^{-3}). However, such a collision would have a kinetic energy of approximately $5 \times 10^{28} \text{ J}$. Since this is not much lower than Titan's gravitational binding energy of $3GM_T/5R_T \approx 2.8 \times 10^{29} \text{ J}$ —a collision with an interplanetary object large enough to cause the change in eccentricity would probably have led to the breakup of Titan.

Lower impact energies (safely below the breakup threshold) could occur for saturnocentric impactors. For example, an object with an apoapsis (Saturn referenced) at Hyperion's distance, and periapsis grazing Titan's orbit, would have a velocity relative to Titan at impact of $\approx 300 \text{ m sec}^{-1}$, requiring a mass of around 0.2 times that of Titan. Thus, an impact origin of the eccentricity still requires a violent collision, perhaps implausibly so.

The alternative solution is a close encounter: a near collision where the bodies exchange momentum by gravitation. Maximum ΔV in such close encounters occurs for the slowest, closest encounter as is well known by spacecraft trajectory planners. In order to constrain the type of encounter required to generate Titan's eccentricity, we first assume that the object had sufficient saturnocentric velocity to escape the saturnian system. Thus, its unperturbed velocity V relative to Titan must have been at least $\sqrt{GM_S/a}(\sqrt{2} - 1)$, or 2.3 km sec^{-1} , and it must have encountered Titan far enough away as not to actually impact (i.e., the miss distance r_p must be greater than R_T). Thus, the eccentricity of the hyperbolic encounter

$$e = 1 + \frac{V^2 r_p}{GM_T} \quad (62)$$

must have been greater than 2.5. The velocity perturbation of the object ΔV_o is simply

$$\Delta V_o = 2V/e \quad (63)$$

or 1.8 km sec^{-1} at most. By conservation of momentum, the perturbation to Titan's orbit ΔV is simply equal to ΔV_o multiplied by the ratio of the object's mass to that of Titan. Thus for the required ΔV of 80 m sec^{-1} , the object must have a mass at least $\frac{1}{2}$ times that of Titan, corresponding again to an object 2000 km in diameter, at least. Once more, such an encounter seems unlikely, although it cannot be ruled out. Further, such an encounter might well have tidally disrupted the object in question, whose fragments may be small enough to be undetected.

Thus, none of the suggested origins seems likely. The origin of the eccentricity and its preservation over time are indeed mysterious. Note, however, that we consider a rheology that depends on frequency as well as on temperature; i.e., the tidal dissipation function Q_μ as given in Eq. (12) depends on both frequency and implicitly on temperature via viscosity. While the tidal frequency is well known, much uncertainty is still connected with the mean interior temperature which we take as 220 K in the present study. Considering the viscosity law for ice given in Eq. (13), it will become apparent that a dramatic enhancement of viscosity, and the related strongly reduced attenuation of tidal strain energy in the interior, is to be expected at mean temperatures close to, e.g., 200 K, which is still conceivable for Titan (Stevenson 1992). Furthermore, the rheological properties of ice will be seriously affected in the presence of volatile contaminants such as ammonia and hydrocarbons alleviating thermal activation of creep and, in turn, rigid rock particles dispersed in the ice increasing creep activation energy (Schubert *et al.* 1986). As it is obvious that the calculation

of Titan's solid dissipation rates suffer from incomplete knowledge of the aforementioned material properties, it is somewhat premature to conclude that the volatile-rich interior structure model is inconsistent with the current eccentricity being primordial.

CONCLUSIONS

We find that solid tidal dissipation rates for the various interior models presented in this study range in value from 8.6×10^9 up to 5.8×10^{10} W in the absence of a global ocean. At least in the current epoch, therefore, interior tidal heating seems to be significantly smaller than the radiogenic component for which Schubert *et al.* (1986) give a range of 4.04 to 5.15×10^{11} W. The removal of radiogenic heat and internal tidal dissipation by crustal heat flow is complex and may involve solid-state convection, conduction, and heat transport by volatiles such as methane in a porous regolith. The various processes that may be at work mean that volcanic and/or tectonic processes cannot be eliminated at present.

Examining several interior and ocean models, we have shown that the current free eccentricity of Titan's orbit is hard to reconcile with the expected tidal dissipation. This is true of not only the dissipation in any reasonable global fluid reservoir, as was noted by Sagan and Dermott (1982), but also for dissipation in the interior, as was noticed by Peale *et al.* (1980). Such considerations would restrict us to Stevenson's (1992) volatile-poor interior model and an ocean, if it exists, with a depth greater than 500 m and almost free of particulates. However, there are several alternative explanations, such as the possibility that Titan's interior has changed significantly over time, the eccentricity has an origin in the more recent past, or, more likely, that our current understanding of the interior of Titan is in error, particularly its past thermal history and mean interior temperature, which controls the solid dissipation via the viscosity.

The Cassini mission will resolve many of the questions raised in this paper. Imaging of surface features by the Huygens probe's imager, and from orbit by near-infrared instrumentation and radar, will identify tectonic or volcanic features. Surface measurements by the Huygens probe (Lorenz 1992b) will allow the measurement of the composition and depth of any liquids at the landing site. Active volcanism will be detected by nightside imaging of Titan by the visible and infrared mapping spectrometer (VIMS). Freshly erupted water-ammonia cryolava at about 170 K will have an emissive flux 20 times higher than the 93 K background in the 5.1- μ m atmospheric window (Baines *et al.* 1992).

Additionally, Doppler tracking of the perturbation of the orbiter's trajectory during the many Titan flybys will allow the determination of the harmonics of Titan's gravi-

tational field. Comoretto *et al.* (1992) suggest that it will be possible to determine the quadrupole coefficient with an accuracy of 1%. Since flybys will be made at different parts of the orbit, Titan's gravitational field will be measured when Titan is subject to different levels of tidal forces. Thus the changing distortion of Titan as a result of tidal forces may be measured, and the real part of the Love numbers estimated.

ACKNOWLEDGMENTS

William McKinnon and Tilman Spohn provided critical reviews which helped greatly to improve this contribution. William Sears was supported by NASA's Graduate Student Researchers Program. Frank Sohl thanks the University of Kiel and the Land Schleswig-Holstein for a postgraduate research grant. Ralph Lorenz acknowledges the support of the UK Science and Engineering Research Council (SERC), now the Particle Physics and Astronomy Research Council (PPARC). Contribution No. 498 Institut für Geophysik, Universität Uid, FRG.

REFERENCES

- BAINES, K. H., R. H. BROWN, D. L. MATSON, R. M. NELSON, B. J. BURATTI, J. P. BIBRING, Y. LANGEVIN, C. SOTIN, A. CARUSI, A. CORADINI, R. N. CLARK, M. COMBES, P. DROSSART, B. SICARDY, D. P. CRUIKSHANK, V. FORMISANO, AND R. JAUMANN 1992. VIMS/Cassini at Titan: Scientific objectives and observational scenarios. In *Proceedings Symposium on Titan, Toulouse, France, 9-12 September 1991*, pp. 137-148. European Space Agency, Noordwijk, The Netherlands.
- BURNS, J. A. 1986. Some background about satellites. In *Satellites* (J. A. Burns and M. S. Matthews, Eds.), pp. 1-38. Univ. of Arizona Press, Tucson.
- CASSEN, P. M., S. J. PEALE, AND R. T. REYNOLDS 1982. Structure and thermal evolution of the Galilean satellites. In *Satellites of Jupiter* (D. Morrison, Ed.), pp. 93-128. Univ. of Arizona Press, Tucson.
- COMORETTO, G., B. BERTOTTI, L. IESS, AND R. AMBROSINI 1992. Doppler experiments with the Cassini radar system. *Nuovo Cimento C*, **15**, 1193-1198.
- CYNN, H. C., S. BOONE, A. KOUMVAKALIS, M. NICOL, AND D. J. STEVENSON 1989. Phase diagram for ammonia-water mixtures at high pressures: Implications for icy satellites. *Proc. Lunar Planet. Sci. Conf. 19th*, pp. 433-441. Lunar and Planetary Science Institute.
- DANBY, J. M. A. 1989. *Fundamentals of Celestial Mechanics*, 2nd ed. William-Bell, Richmond, VA.
- DUBOULOZ, N., F. RAULIN, E. LELLOUCH, AND D. GAUTIER 1989. Titan's hypothesized ocean properties: The influence of surface temperature and atmospheric composition uncertainties. *Icarus* **82**, 81-106.
- ELLSWORTH, K., AND G. SCHUBERT 1983. Saturn's icy satellites: Thermal and structural models. *Icarus* **54**, 490-510.
- FARINELLA, P., P. PAOLICCHI, R. G. STROM, J. S. KARGEL, AND V. ZAPPALA 1990. The fate of Hyperion's fragments. *Icarus* **83**, 375-389.
- FRIEDSON, A. J., AND D. J. STEVENSON 1983. Viscosity of rock-ice mixtures and applications to the evolution of icy satellites. *Icarus* **56**, 1-14.
- GAMMON, P. H., H. KIEFTE, AND M. J. CLOUTER 1983. Elastic constants of ice samples by Brillouin spectroscopy. *J. Phys. Chem.* **87**, 4025-4029.
- GOLDREICH, P., AND S. SOTER 1966. Q in the Solar System. *Icarus* **5**, 375-389.

- GREENBERG, R., AND S. J. WEIDENSCHILLING 1984. How fast do Galilean satellites spin? *Icarus* **58**, 186–196.
- GRIFFITH, C. A. 1993. Evidence for surface heterogeneity on Titan. *Nature* **364**, 511–514.
- JEFFREYS, H. 1925. The flow of water in an inclined channel of rectangular section. *Philos. Mag.* (6) **49**(293), 793–807.
- KAULA, W. M. 1966. *Theory of Satellite Geodesy*. Blaisdell, Waltham, MA.
- KAULA, W. M. 1968. *An Introduction to Planetary Physics: The Terrestrial Planets*. Wiley, New York.
- LAMBECK, K. 1978. Tidal dissipation in the oceans. In *Tidal Friction and the Earth's Rotation* (P. Brosche and J. Sündermann, Eds.), pp. 95–97. Springer-Verlag, New York.
- LARA, L. M. 1993. *Estudio fotoquímico de los componentes neutros de la atmosfera de Titan*. Ph.D. thesis, University of Granada, Spain.
- LARA, L. M., R. D. LORENZ, AND R. RODRIGO 1994. Liquids and solids on the surface of Titan. *Planet. Space Sci.* **42**, 5–14.
- LEMMON, M. T., E. KARKOSCHKA, AND M. TOMASKO 1995. Titan's rotational light-curve. *Icarus* **113**, 27–38.
- LONGMAN, I. M. 1962. A Green's function for determining the deformation of the Earth under surface mass loads, 1. Theory. *J. Geophys. Res.* **67**, 845–850.
- LONGMAN, I. M. 1963. A Green's function for determining the deformation of the Earth under surface mass loads, 2. Computations and numerical results. *J. Geophys. Res.* **68**, 485–496.
- LORENZ, R. 1992a. Gravitational tide in the atmosphere of Titan. In *Proceedings Symposium on Titan, Toulouse, France, 9–12 September 1991*, pp. 119–123. European Space Agency, Noordwijk, The Netherlands.
- LORENZ, R. 1992b. Huygens probe: The surface mission. In *Proceedings Symposium on Titan, Toulouse, France, 9–12 September 1991*, pp. 359–364. European Space Agency, Noordwijk, The Netherlands.
- LORENZ, R. D. 1993. The surface of Titan in the context of ESA's Huygens probe. *ESA J.* **17**, 275–292.
- LOVE, A. E. H. 1927. *A Treatise on the Mathematical Theory of Elasticity*, 4th ed. Dover, New York.
- LUNINE, J. I. 1993. Does Titan have an ocean? A review of current understanding of Titan's surface. *Rev. Geophys.* **31**, 133–149.
- LUNINE, J. I., D. J. STEVENSON, AND Y. L. YUNG 1983. Ethane ocean on Titan. *Science* **222**, 1229–1230.
- LUPU, M. J., AND J. S. LEWIS 1979. Mass-radius relationships in icy satellites. *Icarus* **40**, 157–170.
- MASSEY, W. 1979. *Mechanics of Fluids*, 4th ed. Van Nostrand Reinhold, New York.
- MCKAY, C. P., J. B. POLLACK, J. I. LUNINE, AND R. COURTIN 1993. Coupled atmosphere-ocean models of Titan's past. *Icarus* **102**, 88–98.
- MORRISON, D., T. OWEN, AND L. A. SODERBLOHM 1986. The satellites of Saturn. In *Satellites* (J. A. Burns and M. S. Matthews, Eds.), pp. 764–801. Univ. of Arizona Press, Tucson.
- MUHLEMAN, D. O., A. W. GROSSMAN, M. A. SLADE, AND B. J. BUTLER 1992. The surface of Titan and Titan's rotation: What is radar telling us. *Bull. Am. Astron. Soc.* **24**, 954–955. [Abstract]
- MUNK, W. H., AND G. J. F. MACDONALD 1989. *The Rotation of the Earth: A Geophysical Discussion*, reprint ed. Cambridge Univ. Press, Cambridge.
- PEALE, S. J. 1986. Orbital resonances, unusual configurations and exotic rotation states among planetary satellites. In *Satellites* (J. A. Burns and M. S. Matthews, Eds.), pp. 159–223. Univ. of Arizona Press, Tucson.
- PEALE, S. J., P. CASSEN, AND R. T. REYNOLDS 1980. Tidal dissipation, orbital evolution and the nature of Saturn's inner satellites. *Icarus* **43**, 65–72.
- PELTIER, W. R. 1989. Mantle viscosity. In *Mantle Convection: Plate Tectonics and Global Dynamics* (W. R. Peltier, Ed.), pp. 389–478. Gordon and Breach, New York.
- PLATZMAN, G. W. 1984. Planetary energy balance for tidal dissipation. *Rev. Geophys. Space Phys.* **22**, 73–84.
- POIRIER, J. P. 1982. Rheology of ices: A key to the tectonics of the ice moons of Jupiter and Saturn. *Nature* **299**, 683–688.
- SAGAN, C., AND S. F. DERMOTT 1982. The tides in the seas of Titan. *Nature* **300**, 731–733.
- SCHUBERT, G., T. SPOHN, AND R. T. REYNOLDS 1986. Thermal histories, compositions and internal structure of the moons of the Solar System. In *Satellites* (J. A. Burns and M. S. Matthews, Eds.), pp. 224–292. Univ. of Arizona Press, Tucson.
- SEARS, W. D. 1995. Tidal dissipation in oceans on Titan. *Icarus* **113**, 39–56.
- SEARS, W. D., J. I. LUNINE, AND R. GREENBERG 1993. Equilibrium nonsynchronous rotation of Titan. *Icarus* **105**, 259–262.
- SEGATZ, M., T. SPOHN, M. N. ROSS, AND G. SCHUBERT 1988. Tidal dissipation, surface heat flow, and figure of viscoelastic models of Io. *Icarus* **75**, 187–206.
- SMITH, B. A., L. SODERBLOM, P. BRIDGES, J. INGE, H. MASURSKY, E. SHOEMAKER, R. BEEBE, J. BOYCE, G. BRIGGS, A. BUNKER, S. COLLINS, C. HANSEN, T. JOHNSON, M. DAVIES, G. HUNT, D. MORRISON, T. OWEN, C. SAGAN, J. VERVERKA, R. STROM, AND V. SUOMI 1982. A new look at the Saturn system: The Voyager 2 results. *Science* **215**, 504–537.
- SQUYRES, S. W., AND S. K. CROFT 1986. The tectonics of icy satellites. In *Satellites* (J. A. Burns and M. S. Matthews, Eds.), pp. 293–341. Univ. of Arizona Press, Tucson.
- STEVENSON, D. J. 1992. Interior of Titan. In *Proceedings Symposium on Titan, Toulouse, France, 9–12 September 1991*, pp. 29–33. European Space Agency, Noordwijk, The Netherlands.
- THOMAS, P. C. 1991. Planetary geodesy. *Rev. Geophys. Suppl.* **182**–187.
- TURCOTTE, D. L., AND G. SCHUBERT 1982. *Geodynamics*. Wiley, New York.
- YUNG, Y. L., M. ALLEN, AND J. P. PINTO 1984. Photochemistry of the atmosphere of Titan: Comparison between model and observations. *Astrophys. J. (Suppl. Ser.)* **55**, 465–506.
- ZAHLE, W. 1970. Die Reproduktion gezeitenbedingter Bewegungsvorgänge im Weltozean mittels des hydrodynamisch-numerischen Verfahrens. *Mitt. Inst. Meereskd. Univ. Hamburg* **17**, 1–50.
- ZAHLE, W. 1973. The diurnal K_1 tide in the world ocean—A numerical investigation. *Pure Appl. Geophys.* **109**, 1819–1825.
- ZAHLE, W. 1977. A global hydrodynamic-numerical 1° -model of the ocean-tide; the oscillation system of the M_2 -tide and its distribution of energy dissipation. *Ann. Geophys.* **33**, 31–40.
- ZAHLE, W. 1978. The influence of solid earth deformations on semidiurnal and diurnal oceanic tides. In *Tidal Friction and the Earth's Rotation* (P. Brosche and J. Sündermann, Eds.), pp. 98–124. Springer-Verlag, New York.
- ZAHLE, W. 1980. Mathematical modelling of global interaction between ocean tides and Earth tides. *Phys. Earth Planet. Inter.* **21**, 202–217.
- ZHARKOV, V. N., V. V. LEONTJEV, AND A. V. KOZENKO 1985. Models, figures, and gravitational moments of the Galilean satellites of Jupiter and icy satellites of Saturn. *Icarus* **61**, 92–100.
- ZSCHAU, J. 1978. Tidal friction in the solid Earth: Loading tides versus body tides. In *Tidal Friction and the Earth's Rotation* (P. Brosche and J. Sündermann, Eds.), pp. 62–94. Springer-Verlag, New York.